The International Journal of Advanced Manufacturing Technology (2024) 134:3653–3664
https://doi.org/10.1007/s00170-024-14369-y

ORIGINAL ARTICLE

An innovative process chain for the production of antibiofouling polymer parts using ultrafast laser texturing

Keltoum Oubellaouch[1] · Leonardo Orazi[1,2] · Paola Brun[3] · Giovanni Lucchetta[4] · Riccardo Pelaccia[1] · Marco Sorgato[4]

Received: 30 April 2024 / Accepted: 1 September 2024 / Published online: 6 September 2024

Abstract
Polymers are versatile materials widely used in various industries, with significant applications in biomedicine where biofouling on polymer surfaces presents major health and economic challenges. Biofouling, initiated by bacterial adhesion, can be mitigated by modifying surface properties through laser micro- and nano-texturing, an approach that offers advantages over chemical treatments. This study introduces an economical mass production process for textured polymeric components using injection molding to replicate hierarchical textures. Testing revealed that all textured samples significantly reduced bacterial adhesion compared to untextured surfaces across different designs and bacteria types after 24 h of culture. The study examined factors like wettability, nanoscale roughness, and pattern dimensions to explain these outcomes, comparing them with existing studies. Despite all textured samples showing decreased wettability and roughness, these factors alone did not ensure reduced bacterial adhesion. The most effective anti-adhesive performance was observed in surfaces with parallel ridge patterns, which segmented the surface into isolated areas that limited bacterial interaction and hindered micro-colony formation, highlighting the importance of specific surface patterning in combating biofouling.

Keywords Laser texturing · Replication · Surface functionalization · Bacterial anti-adhesion · Wettability

1 Introduction

In the broad field of biomedical applications, diverse materials serve specific needs in implantable devices, drug delivery, and tissue engineering. Notably, polymers are crucial contributors, distinguished by their exceptional biocompatibility, low costs, flexibility, lightweight properties, and tunability [1]. Their ease of processing and fabrication further enhances adaptability for complex designs and customized applications. However, as the boundaries of biomedical innovation expand, a looming challenge remains the pervasive threat of bacterial infections and the urgent need to fortify surfaces of materials against stealthy colonization by bacteria. This concern has spurred the development of various chemical and physical approaches to create antibacterial surfaces [2].

Antibacterial surfaces, specifically engineered or treated materials, play a pivotal role in inhibiting bacteria growth, survival, or proliferation. The antibacterial property is typically achieved through either a bactericidal effect or an antibiofouling effect [3]. A bactericidal surface can kill bacteria attached to it, while antibiofouling pertains to a material's ability to prevent and inhibit the adhesion and subsequent growth of microorganisms on its surface.

Chemical-based surface coatings with bactericidal properties embrace diverse strategies, such as the use of antimicrobial agents or metallic nanoparticles like silver or copper. Although the former has been extensively employed, the rise of antibiotic-resistant bacteria poses a significant challenge, as these microorganisms may acquire the ability to withstand the effects of antibiotics [4]. Meanwhile, using metallic nanoparticles raises concerns about potential toxicity at

✉ Marco Sorgato
marco.sorgato@unipd.it

[1] Department of Sciences and Methods for Engineering, University of Modena and Reggio Emilia, via Amendola, 42122 Reggio Emilia, Italy

[2] EN&TECH, University of Modena and Reggio Emilia, P.zzale Europa 1, 42124 Reggio Emilia, Italy

[3] Department of Molecular Medicine, University of Padova, via Gabelli 63, 35121 Padua, Italy

[4] Department of Industrial Engineering, University of Padova, via Venezia 1, 35131 Padua, Italy

higher concentrations [5]. Other chemical-based coatings, which are instead designed to confer an antibiofouling effect on surfaces, aiming to prevent and inhibit the adhesion and subsequent growth of microorganisms, are the zwitterionic or poly(ethylene glycol) (PEG). They play a role in enhancing the resilience of surfaces against unwanted microbial attachments [6]. However, a limitation arises when bacteria are already attached, as there is currently no mechanism in place to eliminate them. Moreover, these chemical-based approaches, acknowledged for their efficacy, come with the acknowledgment of being relatively expensive and exhibiting limited effectiveness over time.

Innovative physical methods have emerged to address these challenges and create antibacterial surfaces by meticulously structuring micro- and nano-features. These features are intricately designed to replicate the bactericidal characteristics or antibiofouling properties observed in select plants, insects, and animals, including the cicada, dragonfly, shark skin, and lotus leaves [7]. Diverse techniques have been employed, among them lithography-based methods such as nanoimprint lithography [2] and colloidal lithography [8], as well as reactive ion etching [9], focused ion beam milling [10], and ultrafast laser texturing [11]. Utilizing a mechanical rupturing mechanism, nanospikes [12], nanocones [13], or nano-pillars [14] have demonstrated bactericidal efficacy by inducing physical forces that lead to bacterial protective cell wall rupture or deformation, subsequently causing bacterial cell death.

Instead, physically produced biofouling surfaces are obtained when the adhesion of the bacteria to the surface becomes difficult or impossible. The three primary factors influencing surfaces resistant to bacterial adhesion encompass (i) surface patterning, (ii) surface roughness, and (iii) wettability [15]. Although the hindrance to bacterial adhesion has been extensively studied, a comprehensive analysis of the synergistic effects of these factors remains to be determined. Other factors that should always be considered when designing anti-adhesion surfaces are the types, shapes, and dimensions of bacteria. In broad categorization, bacteria are classified into Gram-negative and Gram-positive groups based on the structural features of their cell walls. Gram-negative bacteria such as *Escherichia coli* (*E. coli*) or *Pseudomonas aeruginosa* (*P. aeruginosa*) are characterized by a thin cell wall, whereas Gram-positive bacteria such as *Staphylococcus aureus* (*S. aureus*) are characterized with a thicker cell wall. In terms of dimensions, the rod-shaped *E. coli* and *P. aeruginosa* exhibit a similar diameter of 0.5 µm, measuring approximately 2 µm and 1.5 µm in length, respectively. In contrast, the spherical *S. aureus* has a diameter of 0.6 µm [16]. In diverse studies [11, 17, 18], it has been shown that surface patterns smaller than the bacteria size reduce the contact area between bacteria and the surface, inhibiting bacterial adhesion and colonization — for example, Epperlein et al. [19] created laser-induced periodic surface structures (LIPSS) on steel with ridges spaced less than 300 nm apart, smaller than *E. coli* dimensions. Resultantly, *E. coli* exhibited reduced adhesion on LIPSS areas compared to polished material. In terms of surface roughness, a negative correlation between roughness (*Ra*) and the anti-adhesion effect is observed for very smooth surfaces ($Ra < 6$ nm), implying those surfaces with smaller Ra exhibit lower antibacterial properties. Conversely, for rougher surfaces ($Ra > 6$ nm), a favorable antibacterial effect is achieved, but surfaces with higher roughness values (submicron and micron roughness) show diminished antibacterial efficacy [15]. The other mechanism influencing bacterial adhesion is surface wettability. Hydrophobic surfaces (exhibiting a water contact angle WCA higher than 90°) or superhydrophobic surfaces (WCA > 150°) have the potential to impede bacterial adhesion. This could be attributed to the trapped air between the features of the hydrophobic surface, leading to a reduction in adhesion force and, consequently, prevention of adhesion [2, 15]. Superhydrophobic microstructure arrays have been shown to prevent the *P. aeruginosa*, *E. coli*, and *S. aureus* biofilm attachment in flow conditions [3]. Using a picosecond laser texturing, San et al. [20] fabricated superhydrophobic surfaces with controllable periodic structures on stainless steel, exhibiting a significant antibiofouling performance. Self-organized structures on titanium surfaces were generated by Fadeeva et al. [21] using femtosecond laser texturing. Both *S. aureus* and *P. aeruginosa* were examined on the obtained superhydrophobic titanium surfaces, revealing that these surfaces efficiently impeded the adhesion of the tested bacteria. Generally, micro- and nanoscale hierarchical structures are known to be highly hydrophobic compared to one-level micro- or nanoscale structures [2]. Nevertheless, various studies have affirmed that predicting bacteria attachment solely based on contact angle measurements is inconclusive. For instance, Cunha et al. [17] engineered anti-adhesion bacterial titanium surfaces through laser texturing, even though the surfaces became hydrophilic after laser treatment.

Among the various physical methods discussed earlier for creating antibacterial surfaces, laser texturing stands out due to its advantages of offering relatively simple, flexible, controllable, and environmentally friendly solutions. This technique is also cost-effective for functionalizing small areas. However, when it comes to mass production of polymeric parts, laser texturing can be time-consuming. Injection molding, on the other hand, is a mass manufacturing process for plastic parts, accommodating a wide range of polymer materials and enabling the production of complex three-dimensional parts. Therefore, the ability to transfer the laser micro- and nano-structures from metallic molds to plastic parts through replication by injection molding is an economical solution, significantly enhancing the productivity of

functionalized polymeric components. The replicability of laser-textured surfaces onto polymer parts through injection molding has been thoroughly explored in previous literature. However, only a limited number of studies have investigated the performance of replicated laser textures on polymer components [22, 23], particularly regarding their anti-adhesion and antifouling properties. Hence, in this investigation, a picosecond laser was used to generate three diverse hierarchical topographies combining micro- and nano-surface features onto steel mold inserts. Subsequently, the micro-injection molding process was employed to replicate the mold insert textures onto components made of polypropylene. The effects of the replicated micro- and nano-textures on the patterned plastic parts were examined and compared to the unpatterned ones, focusing on characteristics such as wettability, roughness, and bacteria retention.

2 Materials and methods

2.1 Picosecond laser treatment

Mold inserts made of 16MnCr5 steel were treated using ultrashort laser micro- and nano-patterning to create hierarchical structures. Prior to laser texturing, the inserts were polished only on the face in contact with the polymer during mold filling, achieving a surface roughness of less than 0.03 µm. Maintaining good roughness is crucial for the successful formation of LIPSS. The laser treatments were conducted using an EKSPLA Atlantic 50 laser system equipped with a High Harmonics Generator and emitting three distinct laser beams at different wavelengths: infrared (IR) at $\lambda = 1064$ nm, green at $\lambda = 532$ nm, and ultraviolet (UV) at $\lambda = 355$ nm. Each of these beamlines generated pulses lasting approximately 10 ps. To direct the laser beams across the workpiece, three Raylase Superscan V galvanometric scanners were employed, along with different F-theta lenses: an 80-mm lens for the IR wavelength, a 75-mm lens for the green wavelength, and a 104-mm lens for the UV wavelength. This configuration allowed for a focused beam with a $1/e^2$ spot diameter of about 10 µm and a working area of 39×39 mm^2, 49×49 mm^2, and 46×46 mm^2, respectively, for the IR, green, and UV beamlines. Furthermore, the laser system is integrated with a three-axis (*X*–*Y*-*Z*) movement system, which allows for flexible adjustment of the worktable's position and the expansion of the operational workspace as required throughout the laser treatment process.

The scanning strategies were developed to create three distinct hierarchical structures by combining two different types of laser textures with different scales: micro- and nanoscale. Regarding the microscale textures, three diverse geometries were designed to be obtained on the polymer part:

- Continuous parallel ridges, each 30 µm wide and spaced 20 µm apart (PR).
- Square-based parallelepipeds, each with a side length of 20 µm and spaced 20 µm apart (S20).
- Square-based parallelepipeds, each with a side length of 60 µm and spaced 20 µm apart (S60).

Negative shapes of these patterns had to be engraved into the inserts to achieve these micro-textures on the polymer parts. For example, to create the first microscale texture, parallel grooves of 30 µm width and spaced 22 µm (as shown in Fig. 1b) were etched over the entire surface of the insert. Similarly, for the second (Fig. 1c) and the third (Fig. 1d) micro-textures, square-based parallelepipeds, spaced 22 µm apart, with side lengths of 20 µm and 60 µm, respectively, were etched from the inserts. For both the grooves and square-based parallelepipeds generation, a 532-nm wavelength laser was used, and to ensure consistent material removal and energy distribution, as can be seen in Fig. 1a, a scanning strategy involving parallel lines spaced 3 µm apart was employed. This strategy was coupled with an appropriate choice of scanning speed and pulse repetition rate to ensure that the pulse distance along the scanlines matched the pulse distance between scanlines, resulting in uniform and precisely controlled micro-textures.

After obtaining the microscale textures on the three inserts, the next step involved creating the nanoscale textures. The chosen nanoscale textures were consistent across all three inserts and involved generating laser-induced periodic surface structures (LIPSS) using a 1064-nm wavelength laser. The scanning strategy for obtaining LIPSS employed parallel lines spaced 4 µm apart, ensuring uniform energy distribution across the material's surface.

Hence, we have a total of three textured inserts with hierarchical strategy, named PRLIPSS (PR + LIPSS), S20LIPSS (S20 + LIPSS), and S60LIPSS (S60 + LIPSS). These designations represent, respectively, the first, the second, and the third micro-textures overlapped with LIPSS nano-texturing. The laser texturing process parameters are summarized in Table 1. As a reference, an unpatterned insert was also considered in this study and coded as a control.

2.2 Micro-injection molding

The test disk is presented in Fig. 2, measuring 15 mm in diameter and 2 mm in thickness. The designed disk features an internal circular cavity, 0.5 mm deep and 8 mm in diameter, on its upper face, intended to locate and contain bacterial cultures. This portion of the disk will come into contact with the textured insert and, consequently, is where the various laser textures will be replicated. As depicted in Fig. 2, a cold runner system was employed, and the gate was positioned on the side of the mold cavity. A

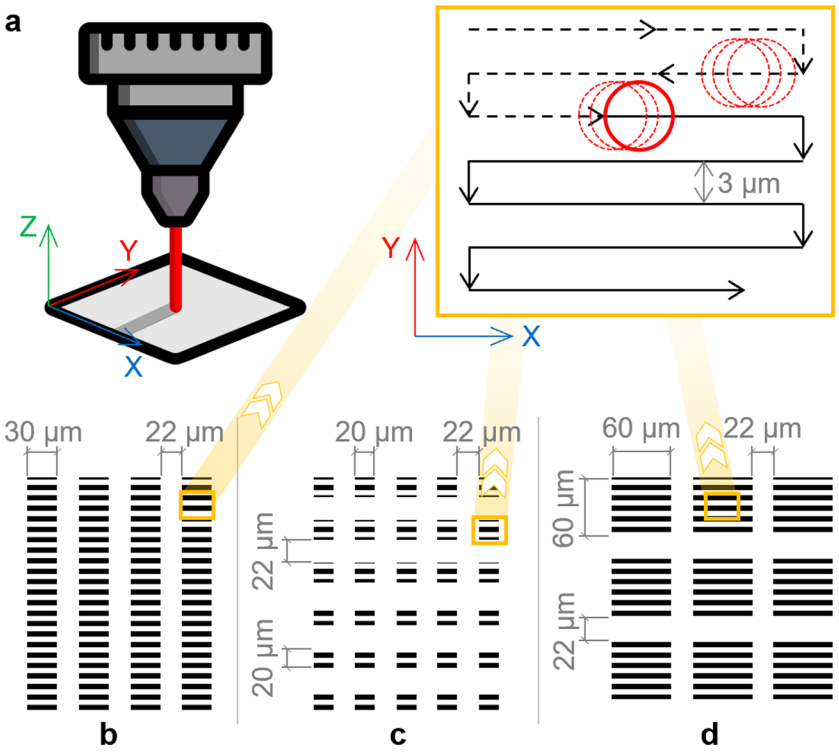

Fig. 1 Schematics of the mold patterning jobs for the three micro-textures. **a** Overlapping laser vectors; **b** continuous parallel ridges (PR); **c** small protrusion 20 µm side (S20); **d** large protrusion 60 µm side (S60)

Table 1 Laser scanning parameters employed for mold micro- and nano-patterning

	Wavelength (nm)	Power (W)	Passes number	Repetition rate (kHz)	Scan speed (mm/s)	Hatch space (µm)	Fluence (J/mm^2)	Dose (J/mm^2)
PR	532	1.1	12	400	1200	3	0.035	0.588
S20	532	1.1	12	400	1200	3	0.035	0.588
S60	532	1.1	12	400	1200	3	0.035	0.588
LIPSS	1064	0.867	1	400	1600	4	0.027	0.033

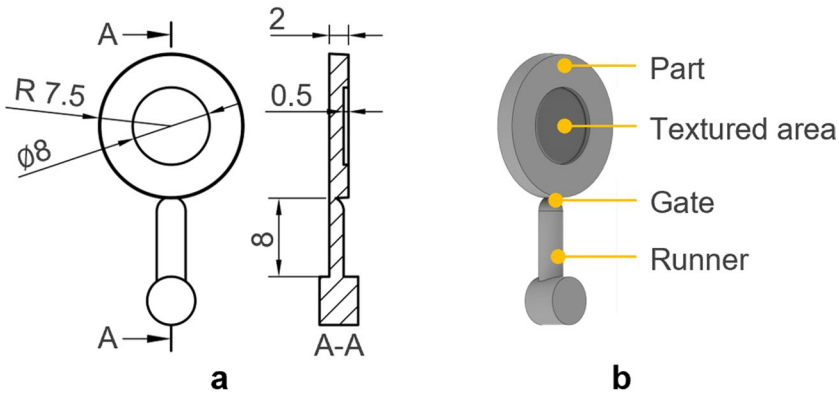

Fig. 2 The injection molded part: **a** drawing with dimensions in millimeters, **b** illustration of the textured area

commercial grade of polypropylene (PP) was employed for its extensive use in automotive and household applications. However, it is worth noting that this material does not possess any specific antibiofouling properties.

The replication of laser textures onto the polypropylene samples was carried out using a micro-injection molding machine (Wittmann Battenfeld, Micro-Power 15). This machine is equipped with a modular mold assembly, which

simplifies the process of mounting various laser-textured inserts. The micro-injection molding process parameters are summarized in Table 2.

2.3 Surface characterization

Qualitative morphological examinations of the unpatterned (control) and patterned mold inserts and their replicated polymer surfaces were conducted using a scanning electron microscope (SEM) to confirm the presence of the generated textures on the mold insert and their successful replication onto the polymer parts. The surfaces were also examined through confocal microscopy (Sensofar Neox), using a 100 × magnification objective with spatial sampling of 140 nm and vertical resolution of 2 nm. For the control geometry and the nano-level of the three samples PRLIPSS, S20LIPSS, and S60LIPSS, a surface of 20×20 μm^2 was evaluated, whereas for the micro-level structures, the analyzed surface was 120×120 μm^2. The arithmetic mean height, *Ra*, measured together with the areal surface roughness parameters: mean hills height, *Rhh*, mean dales depth, *Rdd*, was determined. To characterize the first hierarchical level (the micro-textures), the average height *H* is evaluated as the distance between the planes of maximum and minimum obtained by averaging over the entire analyzed surface.

2.4 Wettability measurement

The wettability assessment of the polymer samples was conducted using the sessile drop method. Two different liquids were utilized: distilled water and a liquid bacterial culture medium. In each test, a 15-μL droplet was carefully deposited. A specially designed dark chamber with an adjustable light source was set up to enhance image quality for this study. A Nikon reflex camera was utilized to photograph the droplet. Subsequently, the acquired images underwent processing through the open-source software ImageJ. A dedicated plugin within the software is applied for drop profile interpolation and the direct calculation of the contact angle. Contact angle measurements were repeated three times for each polymer sample, and the average contact angle was recorded.

Table 2 Micro-injection molding process parameters

Micro-injection molding parameter	Value
Melt temperature	180 °C
Mold temperature	100 °C
Flow rate	205 mm/s
Holding pressure	710 bar
Cooling time	25 s

2.5 Bacterial culture tests of the polymer components

In this research, three varied bacterial strains were selected to assess the efficacy of the suggested configurations: *S. aureus* (designated as strain NCTC 8530), *P. aeruginosa* (designated as strain 109246), and *E. coli* (designated as strain HB101). These strains were acquired from ATCC (LGC Standards, Milan, Italy) and nurtured in Trypticase soy broth (for *S. aureus* and *P. aeruginosa*) or lysogeny broth (for *E. coli*), both supplied by Fisher Scientific. Newly prepared inoculums were cultured for 16 h at 37 °C with continuous shaking at 150 revolutions per minute. After completion of the incubation period, the bacterial cultures' concentration was adjusted to 0.5 McFarland units, equivalent to 1.5×10^8 colony-forming units per milliliter (CFU/mL). The injection molded samples underwent decontamination through a 10-min incubation in ethanol 70% vol/vol, followed by ethanol evaporation under sterile conditions for 16 h. After centrifugation, bacterial cultures were resuspended in growth media to achieve a concentration of 1×10^4 CFU. Subsequently, they were applied to the samples and allowed to incubate at 37 °C for a duration ranging from 30 min to 48 h. Culture plates were placed in a humidification chamber for extended incubation periods to prevent medium evaporation. Following the incubation period, 1 mL of fresh medium was introduced onto the plastic sample surfaces and subjected to vortexing for 5 min to detach all bacterial cells. Subsequently, the samples were transferred to a new sterile tube, appropriately diluted in culture media, and then cultured on agar plates. These plates were then incubated at 37 °C for 16 h, after which bacterial colonies were counted.

3 Results

The SEM images depicted in Fig. 3a, b, and c illustrate the hierarchical structures obtained in the metallic mold inserts, PRLIPSS, S20LIPSS, and S60LIPSS, respectively.

The microstructure's upper and lower levels exhibit LIPSS. Notably, the LIPSS on the upper level are more distinctly defined, benefiting from precise focus during their generation. In Fig. 3d, e, and f, SEM images depict the replicated micro- and nano-structures on the polymer disks, specifically corresponding to PRLIPSS, S20LIPSS, and S60LIPSS, respectively. A qualitative comparison conducted through SEM analysis reveals the successful transfer of the negative design from the mold inserts to the polymer components. This underscores the efficacy of laser texturing on metal surfaces, coupled with replication through injection molding, as an efficient approach to minimizing manufacturing time and costs in producing surfaces tailored for diverse biomedical applications.

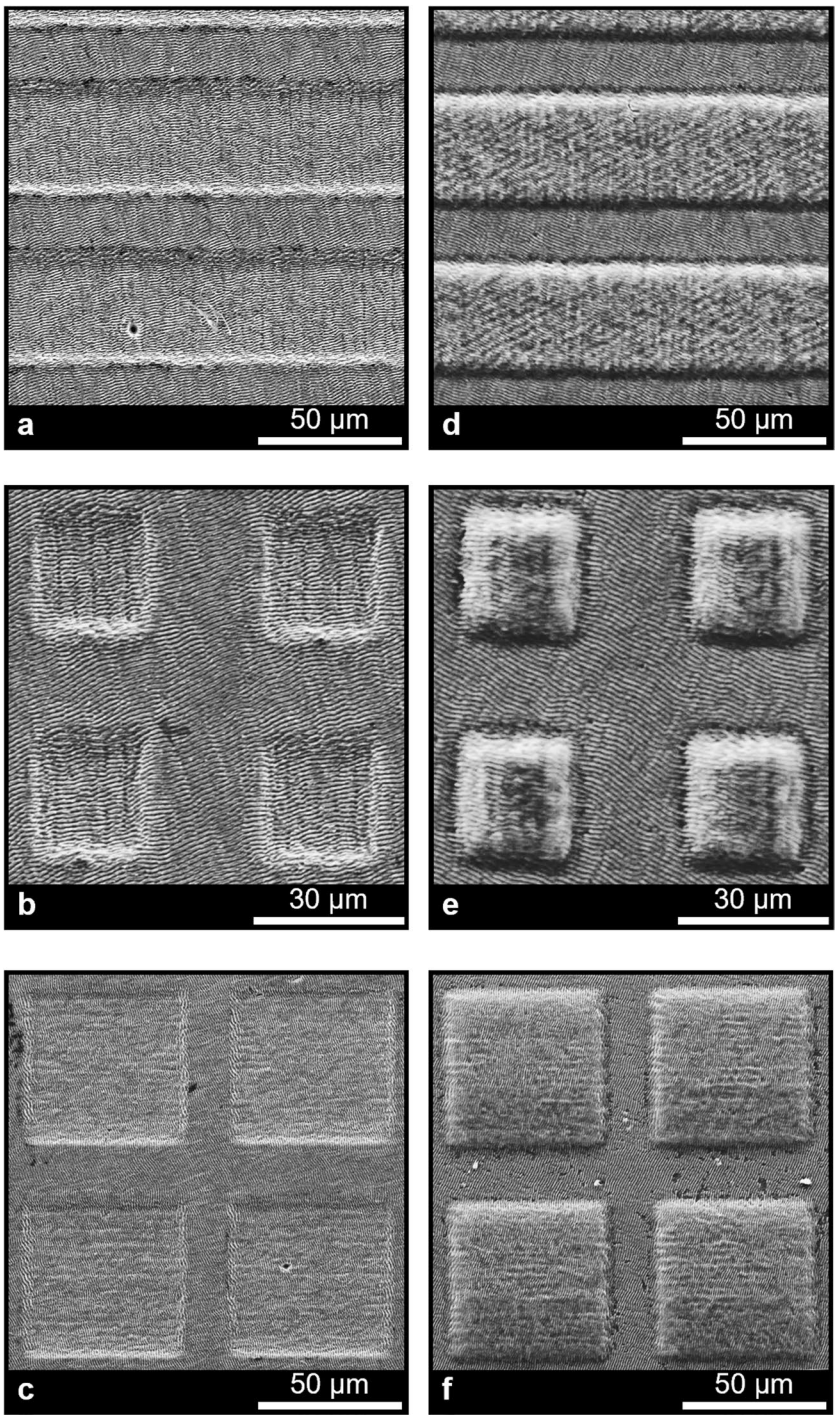

Fig. 3 SEM images of textured mold surfaces (**a**, **b**, **c**) and micro-injection molded replicated polymer parts (**d**, **e**, **f**)

For the quantitative analysis conducted via confocal microscopy, Fig. 4a, b, and c depict images of the PRLIPSS, S20LIPSS, and S60LIPSS polymer components, respectively. Employing Sensoview software, these images were processed to extract various geometric characteristics specific to each surface. A summary of these characteristics is presented in Table 3.

For the control sample and the nano-level structures of the three other samples textured with the hierarchical structures (PRLIPSS, S20LIPSS, and S60LIPSS), the replication quality was evaluated through the comparison of the *Rdd* (mean dales depth) of the mold inserts to the value of the *Rhh* (mean hills height) of the polymeric components, whereas for the analysis of the microscale level of the samples PRLIPSS, S20LIPSS, and S60LIPSS, the average height *H* spanning from the lowest to the highest planes of the mold inserts was compared to that of their corresponding replicated samples. The comparison for all

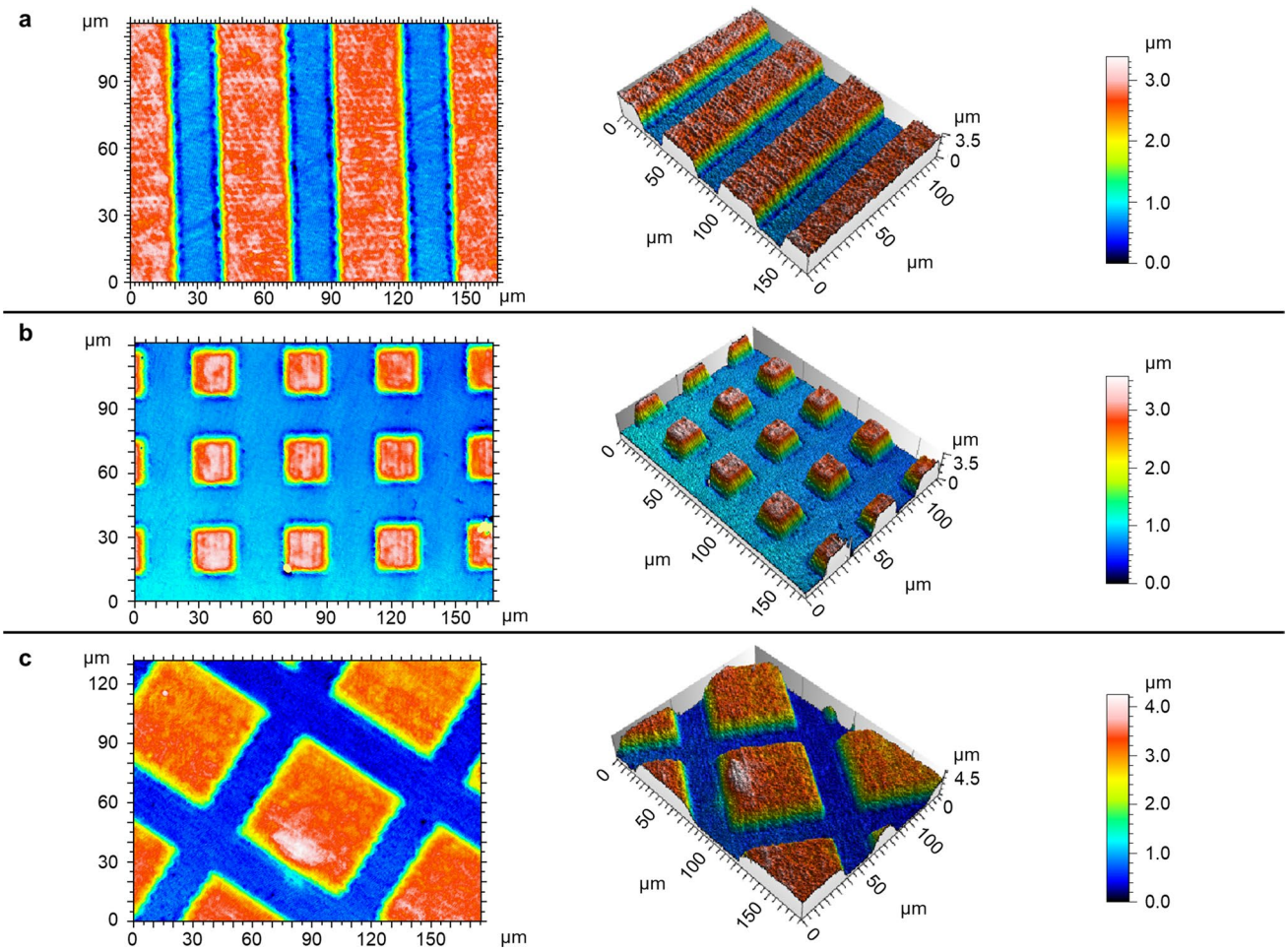

Fig. 4 The topographies acquired using the confocal microscope of (**a**) PRLIPSS, (**b**) S20LIPSS, (**c**) S60LIPSS

Table 3 Surface topography values measured using the confocal microscope

Parameter	Control		PRLIPSS		S20LIPSS		S60LIPSS	
	Mold	PP	Mold	Polymer	Mold	Polymer	Mold	Polymer
H (µm)	-	-	2.9	2.8	2.4	2.4	3.4	3.5
Ra (nm)	426	408	15	12	15	12	15	12
Rhh (nm)	61	59	6	5	5	4	7	5
Rdd (nm)	63	63	6	4	5	4	7	6

structures revealed highly comparable values between metallic mold inserts and their negative replicas in the polymeric samples. Additionally, although the roughness values (*Ra*) were slightly higher on the insert, they remained comparable between the insert and the polymer. This underscores the precision of injection molding as a replication process.

Figure 5a and b illustrate the results regarding contact angle measurements using water and bacterial culture liquid, respectively. These results vividly demonstrate that laser texturing has led to a remarkable variation in the wetting characteristics of the examined surfaces. Notably, the unpatterned polymer demonstrates a hydrophilic behavior with a contact angle of less than 90°, whether measured with water or bacterial culture liquid. In contrast, all patterned polypropylene surfaces exhibit highly hydrophobic characteristics, evidenced by contact angles exceeding $118° \pm 2°$ with water or $109° \pm 2°$ with bacterial culture liquid. Notably, across all textured parts, the evaluation of wettability using water consistently yields higher contact angles compared to the bacterial culture liquid.

The percentage of deceased bacteria, as depicted in Fig. 6 for each replicated textured polymer surface, is determined

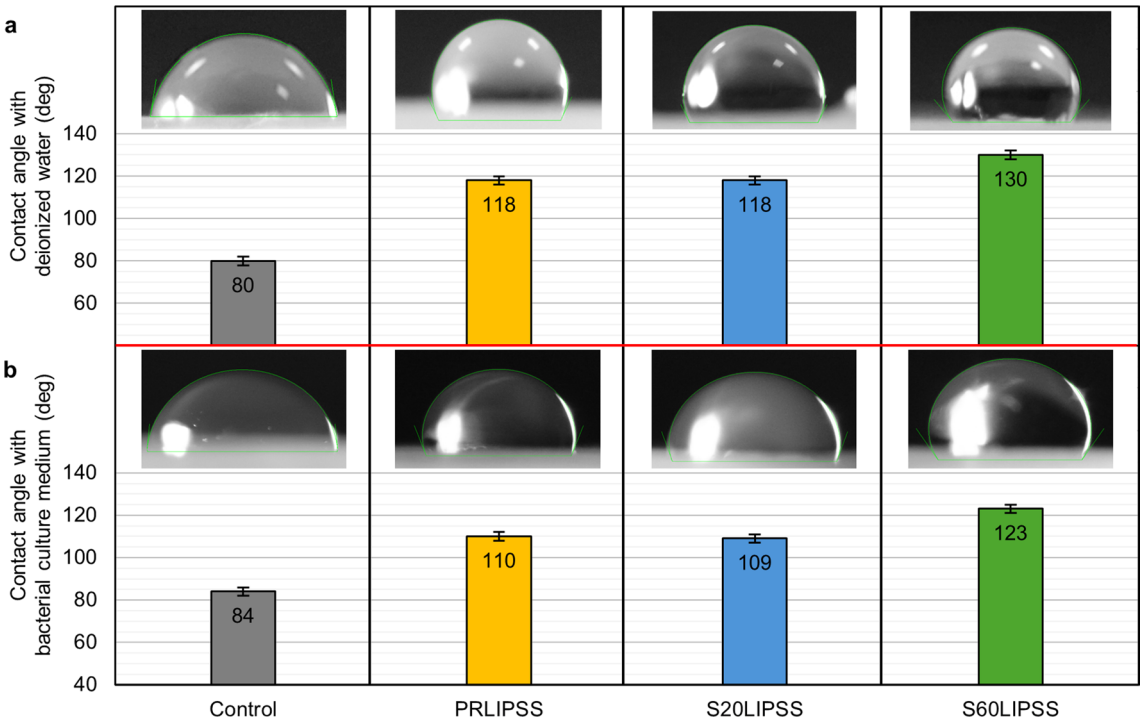

Fig. 5 **a** Contact angle measurement with deionized water. **b** Contact angle measurement with bacterial culture liquid

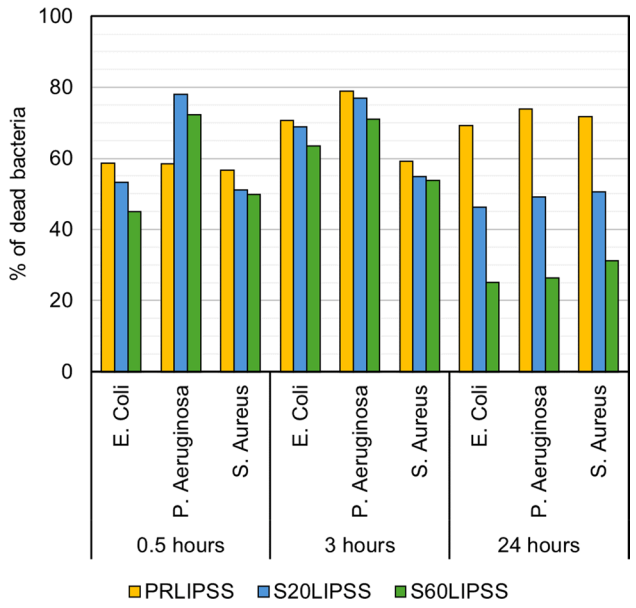

Fig. 6 Antibacterial performance evolution of the three proposed hierarchical textures compared to the control surface

by comparing the number of live bacteria on the textured polymer surface to that on the control polymer surface. In general, it is evident that all the replicated textured polymer surfaces successfully increase the proportion of dead bacteria compared to the control polymer surface. Regardless of the bacterial type, the proposed hierarchical structures effectively reduced bacterial colonization, showcasing the versatility of the proposed designs. Figure 7a, b, and c illustrate bacterial growth curves for all samples (control, PRLIPSS, S60LIPSS, S20LIPSS) corresponding to *P. aeruginosa*, *E. coli*, and *S. aureus*, respectively, over the observation period of 24 h. The growth curves of all studied bacteria on the control surface exhibited the typical curve shape with three distinct phases: lag, exponential, and stationary. Conversely, there is a reduced increase in the bacterial count over time for the other replicated polymer surfaces, and the growth curves do not exhibit the same pronounced typical shape.

4 Discussion

A comprehensive understanding of bacterial adhesion mechanisms is essential for designing successful surfaces that can effectively inhibit bacterial adhesion. In this work, using different scanning strategies, a picosecond laser texturing was used to generate three different hierarchical structures onto metallic inserts that were replicated on polypropylene polymer using micro-injection molding. As discussed in Section 1, surface roughness is a key factor influencing surface adhesion. Previous studies have demonstrated that surfaces with nanoscale roughness ($Ra > 6$ nm) tend to inhibit bacterial adhesion, and an increase in roughness values corresponds to a rise in bacterial adhesion [15]. Consistent

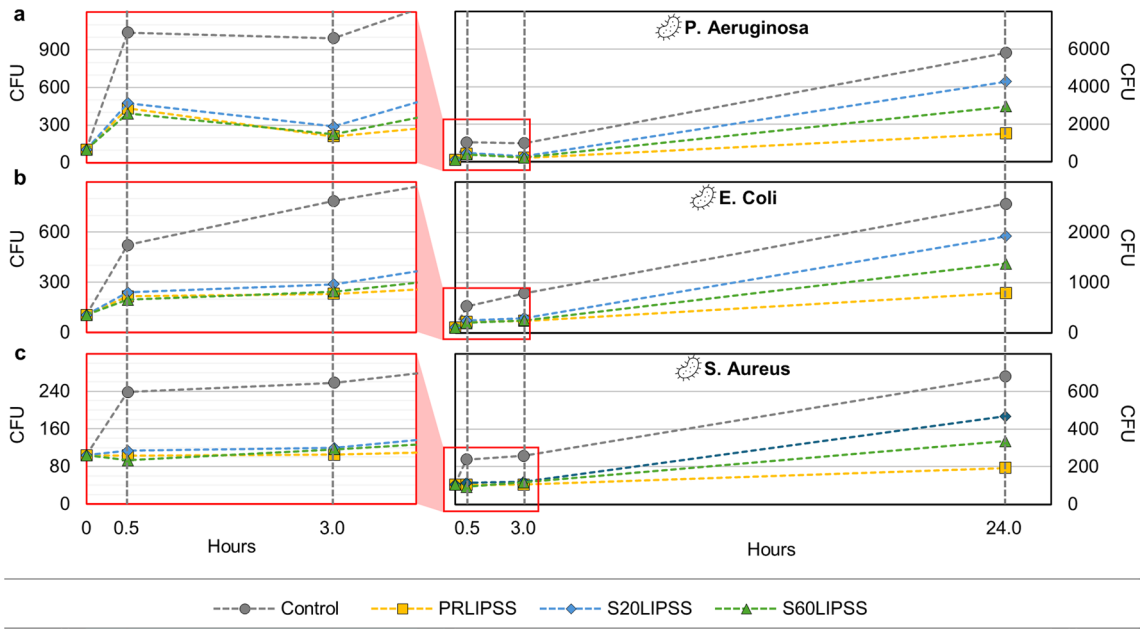

Fig. 7 Growth curves for (**a**) *P. aeruginosa*, (**b**) *E. coli*, and (**c**) *S. aureus* of the control and three hierarchical textures (PRLIPSS, S20LIPSS, S60LIPSS)

with these findings, our results reveal that the patterned samples, which exhibit approximately 12 nm of roughness (in terms of *Ra*), displayed antibacterial properties compared to the unpatterned sample, with a higher roughness value of almost 408 nm (in terms of *Ra*). The wettability of surfaces is another crucial factor influencing bacterial adhesion. It is widely acknowledged that reduced wettability leads to decreased bacterial adhesion. Interestingly, all patterned samples exhibited highly hydrophobic behavior compared to the unpatterned polypropylene, demonstrating a hydrophilic tendency. Contrary to the assumption that a higher contact angle necessarily corresponds to enhanced bacterial anti-adhesion behavior, our results unveil nuances in this relationship. Specifically, the S60LIPSS sample, boasting the highest contact angle (130° with water), exhibited increased bacterial growth compared to PRLIPSS, which had a lower contact angle of approximately 118°. Furthermore, while PRLIPSS and S20LIPSS samples displayed identical contact angles, the bacterial growth in S20LIPSS was unexpectedly high. These observations highlight the intricate interplay between surface wettability and bacterial adhesion, emphasizing that a higher contact angle does not uniformly guarantee superior anti-adhesion properties. This aligns with Francone et al.'s findings [2], emphasizing that bacterial attachment cannot be solely predicted by contact angle measurements. Higher contact angles were observed with nanospikes on top of micropillars, but this configuration exhibited greater bacterial attachment than nanospikes at the bottom of the micropillars. An alternative explanation may arise from the timing of contact angle measurements conducted shortly after droplet deposition (within seconds or minutes). This timing tends to stabilize the Cassie-Baxter state. Conversely, during the bacterial culture tests, the samples were immersed in the liquid for an extended period (hours), leading to the observation and confirmation of the Wenzel state [24].

In the zoomed sections of Fig. 7, during the initial phase of the adhesion process known as initial adhesion, there is a decrease in adhesion over time. One factor known to regulate this initial bacterial growth is hydrophobic interactions [25]. This could explain why the design with the highest hydrophobic behavior exhibits the lowest bacterial growth during this initial adhesion phase.

Examining Fig. 7a, b, and c, it is evident that, among the investigated bacteria, *S. aureus* consistently displayed the lowest bacterial growth across all examined samples, with a CFU nearly ten times smaller than that of *P. aeruginosa* and approximately five times smaller than the growth of *E. coli*. Unlike the other two bacteria studied, *S. aureus* is a Gram-positive bacterium with a spherical shape. Due to this spherical form, repulsive hydrophobic forces have successfully reduced its adhesion to the surface. Another contributing factor may be that *E. coli* and *P. aeruginosa* are motile bacteria equipped with flagella, enabling them to navigate through the liquid culture to locate suitable colonization sites [26, 27]. Despite the static nature of the culture tests, these bacteria can move to find an appropriate surface for habitation.

Moreover, flagella's existence can serve as a connective link between features, creating a mesh that enhances the

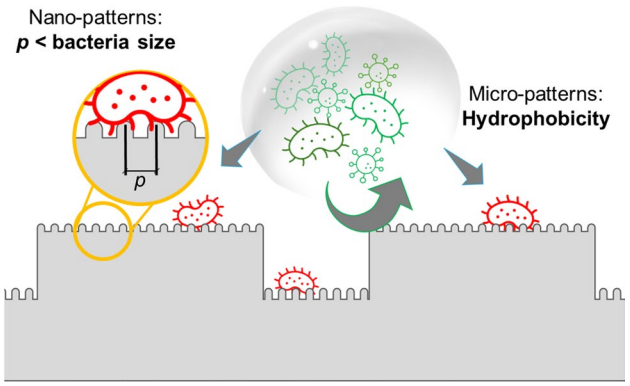

Fig. 8 The designed hierarchical structures have a dual effect: hydrophobicity and nano-texture size smaller than the bacteria size

attachment of more cells [28]. In contrast, *S. aureus* is a non-motile bacterium lacking flagella [29]. In static conditions, if the surface exhibits minimal anti-adhesion behavior, *S. aureus* may fail to adhere to the surface, resulting in death.

Bacterial adhesion necessitates a contact area exceeding the size of the bacteria. In a study by Epperlein et al. [19], LIPSS were fabricated on a steel surface, with ridges spaced less than 300 nm apart. With a diameter of 500 nm, *E. coli* was incapable of adhering within the LIPSS — conversely, Hsu et al. [30] designed linear structures spaced at 1 µm, exceeding the width of the tested bacterium (500 nm). Their findings revealed that bacteria could align themselves with these structures. Similarly, Graham et al. [31], in microscopic observations of cell-surface attachment, noted *E. coli* aligning between lines. This alignment is influenced by bacterial shape, with rod-like bacteria showing a greater propensity to align within linear structures. In our study, replicated polypropylene samples had LIPSS ridge distances smaller than 450 nm. All tested bacteria (*E. coli*, *P. aeruginosa*, *S. aureus*) had diameters larger than 500 nm, making adhesion challenging. Consequently, CFU for treated samples was lower than that for unpatterned samples. Figure 8 illustrates the designed hierarchical textures, characterized by dual-scale textures. The microscale textures contribute to hydrophobicity, creating a surface that resists bacterial adhesion due to repulsive hydrophobic forces. On the other hand, the nanoscale textures, specifically the LIPSS with ridges spaced at distances smaller than the size of the bacteria, hinder their adhesion to the surface. This dual-scale texturing approach effectively mitigates bacterial adhesion and enhances the overall performance of the treated samples.

In addition to the factors discussed so far, bacterial adhesion hinges on the ability to produce a sufficient quantity of extracellular polymeric substances (EPS) matrix [21]. This matrix plays a crucial role in anchoring bacteria to surfaces, providing an encasement that shields them against removal [31]. The ease and adequacy of EPS production come into play when bacteria organize into micro-colonies [32], formed through their mutual encounters. As elucidated in various studies [32–34], bacteria predominantly colonize the valleys of micro-textures, rarely congregating on their summits. Consequently, micro-textures can be viewed as barriers hindering bacterial interactions and micro-colony formation. When comparing S20LIPSS to S60LIPSS, the former is characterized by smaller barriers, presenting a higher likelihood for bacteria to encounter each other and form micro-colonies. Conversely, PRLIPSS, distinguished by continuous parallel ridges, demonstrates the most effective performance. This can be attributed to the microstructure effectively partitioning the surface into zones that restrict bacterial interactions, impeding micro-colony formation and EPS matrix development.

5 Conclusion

In this study, a novel and cost-effective process chain was developed for the first time, enabling the production of polymer parts with surfaces characterized by reduced bacterial adhesion. This process chain involves the texturing of the mold using picosecond laser techniques, with subsequent replication of these textures onto polymer parts through the injection molding process. Three hierarchical micro- and nano-textures were proposed, and regardless of the bacterial type, these hierarchical structures consistently demonstrated an effective reduction in bacterial colonization compared to untreated samples, showing the versatility of the proposed designs.

Both the wettability and nanoscale roughness (assessed at the top or between the micro-features) were reduced in the patterned samples. The generated micro-features made the surface hydrophobic, creating repulsive hydrophobic forces that impede bacterial adhesion. When the surface's hydrophobicity fails to inhibit bacterial adhesion, the developed designs incorporate LIPSS structures at the top of the micro-features or between them. The LIPSS have a dual effect; on the one hand, they exhibit reduced roughness compared to untreated surfaces, reducing support for bacterial adhesion. On the other hand, the width of the valleys of the replicated LIPSS is smaller or comparable to the size of bacteria, making their adhesion to the surface more challenging.

In addition to hydrophobicity, the micro-features can be viewed as barriers preventing bacteria from coming into contact with each other. Consequently, this impedes the formation of micro-colonies and, subsequently, the EPS matrix. Surfaces with longer and larger barriers, effectively partitioning the surface into zones that limit bacterial interactions, have demonstrated superior performance.

Author contribution Keltoum Oubellaouch: methodology, investigation, writing — original draft. Leonardo Orazi: writing — review and editing, supervision, funding acquisition. Paola Brun: validation, investigation. Giovanni Lucchetta: conceptualization, writing — review and editing, supervision. Riccardo Pelaccia: methodology, investigation. Marco Sorgato: conceptualization, formal analysis, writing — review and editing, supervision.

Funding Open access funding provided by Università degli Studi di Padova within the CRUI-CARE Agreement. The activities were partially funded under the National Recovery and Resilience Plan (NRRP), Mission 04, Component 2, Investment 1.5 – NextGenerationEU, Call for tender n. 3277, dated 30/12/2021. Award Number: 0001052 dated 23/06/2022.

Declarations

Competing interests The authors declare no competing interests.

References

1. Kumara SPSNBS, Senevirathne SWMAI, Mathew A, Bray L, Mirkhalaf M, Yarlagadda PKDV (2023) Progress in nanostructured mechano-bactericidal polymeric surfaces for biomedical applications. Nanomaterials 13(20):2799. https://doi.org/10.3390/nano13202799
2. Francone A, Merino S, Retolaza A, Ramiro J, Alves SA, de Castro JV, Neves NM, Arana A, Marimon JM, Sotomayor Torres CM, Kehagias N (2021) Impact of surface topography on the bacterial attachment to micro- and nano-patterned polymer films. Surf Interfaces 27:101494. https://doi.org/10.1016/j.surfin.2021.101494
3. Hasan J, Crawford RJ, Ivanova EP (2013) Antibacterial surfaces: the quest for a new generation of biomaterials. Trends Biotechnol 31(5):295–304. https://doi.org/10.1016/j.tibtech.2013.01.017
4. Baptista PV, McCusker MP, Carvalho A, Ferreira DA, Mohan NM, Martins M, Fernandes AR (2018) Nano-strategies to fight multidrug resistant bacteria-'a battle of the titans.' Front Microbiol 9:1441. https://doi.org/10.3389/fmicb.2018.01441
5. Slavin YN, Asnis J, Häfeli UO, Bach H (2017) Metal nanoparticles: understanding the mechanisms behind antibacterial activity. J Nanobiotechnol 15(1):65. https://doi.org/10.1186/s12951-017-0308-z
6. Cao Z, Mi L, Mendiola J, Ella-Menye JR, Zhang L, Xue H, Jiang S (2012) Reversibly switching the function of a surface between attacking and defending against bacteria. Angew Chem Int Ed 51(11):2602–2605. https://doi.org/10.1002/anie.201106466
7. Jaggessar A, Shahali H, Mathew A, Yarlagadda PKDV (2017) Bio-mimicking nano and micro-structured surface fabrication for antibacterial properties in medical implants. J Nanobiotechnol 15(1). https://doi.org/10.1186/s12951-017-0306-1
8. Liu W, Liu X, Fangteng J, Wang S, Fang L, Shen H, Xiang S, Sunb H, Yang B (2014) Bioinspired polyethylene terephthalate nanocone arrays with underwater superoleophobicity and antibioadhesion properties. Nanoscale 6(22):13845–13853. https://doi.org/10.1039/C4NR04471A
9. Anindo R, Kaushik C (2022) Bactericidal anisotropic nanostructures on titanium fabricated by Maskless dry etching. ACS Appl Nano Mater. https://doi.org/10.1021/acsanm.2c00555
10. Wu SE, Huang YW, Hsueh TH, Liu CP (2008) Fabrication of nanopillars comprised of InGaN/GaN multiple quantum wells by focused ion beam milling. Jpn J Appl Phys 47(6):4906–4908. https://doi.org/10.1143/JJAP.47.4906
11. Lutey AH, Gemini L, Romoli L, Lazzini G, Fuso F, Faucon M, Kling R (2018) Towards laser-textured antibacterial surfaces. Sci Rep 8(1):10112. https://doi.org/10.1038/s41598-018-28454-2
12. Sorgato M, Brun P, Savio E, Lucchetta G (2023) A process chain for the mass production of nanopatterned bactericidal plastic parts. CIRP Ann 72(1):477–480. https://doi.org/10.1016/j.cirp.2023.04.014
13. Hazell G, Fisher LE, Murray WA, Nobbs AH, Su B (2018) Bioinspired bactericidal surfaces with polymer nanocone arrays. J Colloid Interface Sci 528:389–399. https://doi.org/10.1016/j.jcis.2018.05.096
14. Pogodin S, Jafar H, Baulin VA, Webb HK, Truong VK, Nguyen THP, Boshkovikj V, Fluke CJ, Waston GS, Waston JA, Crawford RJ, Ivanova EP (2013) Biophysical model of bacterial cell interactions with nanopatterned cicada wing surfaces. Biophys J 104(4):835–840. https://doi.org/10.1016/j.bpj.2012.12.046
15. Yang K, Shi J, Wang L, Chen Y, Liang C, Yang L, Wang LN (2022) Bacterial anti-adhesion surface design: Surface patterning, roughness and wettability: a review. J Mater Sci Technol 99:82–100. https://doi.org/10.1016/j.jmst.2021.05.028
16. Maleki E, Mirzaali MJ, Guagliano M, Bagherifard S (2021) Analyzing the mechano-bactericidal effect of nano-patterned surfaces on different bacteria species. Surf Coat Technol 408:126782. https://doi.org/10.1016/j.surfcoat.2020.126782
17. Cunha A, Elie AM, Plawinski L, Serro AP, Botelho do Rego AA, Almeida A, Urdaci MC, Durrieu MC, Vilar R (2016) Femtosecond laser surface texturing of titanium as a method to reduce the adhesion of Staphylococcus aureus and biofilm formation. Appl Surface Sci 360:485–493. https://doi.org/10.1016/j.apsusc.2015.10.102
18. Lorenzetti M, Dogša I, Stošicki T, Stopar D, Kalin M, Kobe S, Novak S (2015) The influence of surface modification on bacterial adhesion to titanium-based substrates. ACS Appl Mater Interfaces 7:1644–1651. https://doi.org/10.1021/am507148n
19. Epperlein N, Menzel F, Schwibbert K, Koter R, Bonse J, Sameith J, Krüger J, Toepel J (2017) Influence of femtosecond laser produced nanostructures on biofilm growth on steel. Appl Surf Sci 418:420–424. https://doi.org/10.1016/j.apsusc.2017.02.174
20. Sun K, Yang H, Xue W, He A, Zhu D, Liu W, Adeyemi K, Cao Y (2018) Anti-biofouling superhydrophobic surface fabricated by picosecond laser texturing of stainless steel. Appl Surf Sci 436:263–267. https://doi.org/10.1016/j.apsusc.2017.12.012
21. Fadeeva E, Truong VK, Stiesch M, Chichkov BN, Crawford RJ, Wang J, Ivanova EP (2011) Bacterial retention on superhydrophobic titanium surfaces fabricated by femtosecond laser ablation. Langmuir 27(6):3012–3019. https://doi.org/10.1021/la104607g
22. Romano J-M, Garcia-Giron A, Penchev P, Gulcur M, Whiteside BR, Dimov S (2020) Lotus-leaf inspired surfaces: hydrophobicity evolution of replicas due to mechanical cleaning and mold wear. J

Micro Nano-Manuf 8(1):010913. https://doi.org/10.1115/1.4046097
23. Romano J-M, Gulcur M, Garcia-Giron A, Martinez-Solanas E, Whiteside BR, Dimov SS (2019) Mechanical durability of hydrophobic surfaces fabricated by injection moulding of laser-induced textures. Appl Surf Sci 476:850–860. https://doi.org/10.1016/j.apsusc.2019.01.162
24. Arunachalam S, Das R, Nauruzbayeva J, Domingues EM, Mishra H (2019) Assessing omniphobicity by immersion. J Colloid Interface Sci 534:156–162. https://doi.org/10.1016/j.jcis.2018.08.059
25. Kim S et al (2015) Nanostructured multifunctional surface with antireflective and antimicrobial characteristics. ACS Appl Mater Interfaces 7(1):326–331. https://doi.org/10.1021/am506254r
26 Nakamura S, Minamino T (2019) Flagella-driven motility of bacteria. Biomolecules 9(7):279. https://doi.org/10.3390/biom9070279
27. Khan F, Pham DTN, Oloketuyi SF, Kim Y-M (2020) Regulation and controlling the motility properties of Pseudomonas aeruginosa. Appl Microbiol Biotechnol 104(1):33–49. https://doi.org/10.1007/s00253-019-10201-w
28. Friedlander RS, Vlamakis H, Kim P, Khan M, Kolter R, Aizenberg J (2013) Bacterial flagella explore microscale hummocks and hollows to increase adhesion. Proc Natl Acad Sci USA 110(14):5624–5629. https://doi.org/10.1073/pnas.1219662110
29. Samad T, Billings N, Birjiniuk A, Crouzier T, Doyle PS, Ribbeck K (2017) Swimming bacteria promote dispersal of non-motile staphylococcal species. ISME J 1(8):1933–1937. https://doi.org/10.1038/ismej.2017.23
30. Hsu LC, Fang J, Borca-Tasciuc DA, Worobo RW, Moraru CI (2013) Effect of micro- and nanoscale topography on the adhesion of bacterial cells to solid surfaces. Appl Environ Microbiol 79(8):2703–2712. https://doi.org/10.1128/AEM.03436-12
31 Graham MV, Mosier AP, Kiehl TR, Kaloyeros AE, Cady NC (2013) Development of antifouling surfaces to reduce bacterial attachment. Soft Matter 9(27):6235. https://doi.org/10.1039/C3SM50584G
32. Chang Y-R, Weeks ER, Ducker WA (2018) Surface topography hinders bacterial surface motility. 10(11):9225-9234https://doi.org/10.1021/acsami.7b16715
33. Meel C, Kouzel N, Oldewurtel ER, Maier B (2012) Three-dimensional obstacles for bacterial surface motility. Small 8(4):530–534. https://doi.org/10.1002/smll.201101362
34. Vasudevan R, Kennedy AJ, Merritt M, Crocker FH, Baney RH (2014) Microscale patterned surfaces reduce bacterial fouling-microscopic and theoretical analysis. Colloids Surf B 117:225–232. https://doi.org/10.1016/j.colsurfb.2014.02.037